The Plasma Membrane Calcium ATPase MCA-3 is Required for Clathrin-Mediated Endocytosis in Scavenger Cells of *Caenorhabditis elegans*

Ewa M. Bednarek[1,2], Lara Schaheen[3], Jayne Gaubatz[1], Erik M. Jorgensen[1,*] and Hanna Fares[3]

[1]Department of Biology and Howard Hughes Medical Institute, University of Utah, Salt Lake City, UT 84112, USA
[2]Current address: Friedrich Miescher Institute, 4058 Basel, Switzerland
[3]Department of Molecular and Cellular Biology, University of Arizona, Tucson, AZ 85721, USA
*Corresponding author: Erik M. Jorgensen, jorgensen@biology.utah.edu

Plasma membrane Ca^{2+} ATPases (PMCAs) maintain proper intracellular Ca^{2+} levels by extruding Ca^{2+} from the cytosol. PMCA genes and splice forms are expressed in tissue-specific patterns in vertebrates, suggesting that these isoforms may regulate specific biological processes. However, knockout mutants die as embryos or undergo cell death; thus, it is unclear whether other cell processes utilize PMCAs or whether these pumps are largely committed to the control of toxic levels of calcium. Here, we analyze the role of the PMCA gene, *mca-3*, in *Caenorhabditis elegans*. We report that partial loss-of-function mutations disrupt clathrin-mediated endocytosis in a class of scavenger cells called coelomocytes. Moreover, components of early endocytic machinery are mislocalized in *mca-3* mutants, including phosphatidylinositol-4,5-bisphosphate, clathrin and the Eps15 homology (EH) domain protein RME-1. This defect in endocytosis in the coelomocytes can be reversed by lowering calcium. Together, these data support a function for PMCAs in the regulation of endocytosis in the *C. elegans* coelomocytes. In addition, they suggest that endocytosis can be blocked by high calcium levels.

Key words: calcium, clathrin, Cup, endocytosis, inhibition, MCA-3, phosphatidylinositol-4,5-bisphosphate, PI(4,5)P$_2$, plasma membrane calcium ATPase, PMCA

The concentration of calcium is about 10 000-fold higher outside than inside cells. Extracellular calcium is around 2.5 mM, whereas intracellular calcium is quite low; for example, in *Drosophila* neurons calcium is at 23 nM (1). Thus, opening of calcium channels causes profound local increases in cytosolic Ca^{2+}, which then initiate signaling cascades within the cell (2). Aberrant calcium increases can inappropriately activate second messenger signaling cascades or can initiate necrotic or programmed cell death (3). Thus, after influx, calcium levels in the cell must be rapidly restored to maintain cellular homeostasis. Extrusion of cytoplasmic calcium is accomplished by two plasma membrane-localized systems: sodium–calcium exchangers (NCXs) and plasma membrane Ca^{2+} ATPases (PMCAs) (4).

Plasma membrane calcium ATPases play essential roles in capping cytosolic calcium levels (5). A chronically high level of calcium is very dangerous to cell viability because it can initiate programmed or degenerative cell death (3). The phenotypes of PMCA knockouts are consistent with an initiation of cell death caused by chronic levels of calcium (4). For example, lack of the ubiquitous pump PMCA4 causes increased apoptosis of particular smooth muscles (6). Inhibition or mutations of the neuronally expressed PMCA2 can lead to cell death of hair cells or spinal cord neurons (6,7). In the absence of PMCA1 function, mutants die as embryos before implantation (6). In addition, PMCAs are a target of caspases, and their caspase-mediated cleavage has been shown to promote apoptosis (8). Thus, the PMCAs are likely to be important for pumping down calcium when it reaches toxic levels in the cell.

There is evidence that PMCAs can be activated under nonlethal calcium concentrations to tune calcium-sensitive cellular processes. First, calcium ATPases have a higher affinity for calcium than the NCXs, and are therefore poised to respond to lower concentrations of calcium (9). Second, the diversity of isoforms and their specific subcellular localizations suggest that different PMCAs are specialized to regulate different biological functions. Alternative splicing among these isoforms determines calcium sensitivity or inhibition by protein kinase C (4). Third, at least two PMCAs are likely to regulate biological processes. Murine PMCA4 is necessary for sperm motility (6,10); it is possible that this calcium ATPase modulates calcium dynamics in the sperm tail thereby influencing motor activity. In the smooth muscle of the bladder, PMCA1 and PMCA4 control the relaxation rate and thus maintain the contraction–relaxation cycle (11). Fourth, computational modeling of inner hair cell physiology suggests that calcium dynamics in these cells are likely to be shaped in part by the calcium ATPase PMCA2a (12,13). However, this proposal remains to be confirmed *in vivo*. Thus, it is highly probable that calcium ATPases play important roles in tuning calcium levels for many cell processes. However, identifying

which cell processes rely on PMCA function is difficult using genetic techniques because the phenotypes associated with null mutations in these genes are often too severe. Thus, isolation of weak mutations may be important for the analysis of PMCA function in cells.

Here we demonstrate that hypomorphic mutations in a PMCA gene in the nematode *Caenorhabditis elegans* disrupt endocytosis. These mutations were isolated in a genetic screen for mutants defective for endocytosis by specialized scavenger cells (14). These six scavenger cells, called coelomocytes, are distributed in the body cavity. Coelomocytes have a high rate of continuous endocytosis and can rapidly clear fluid phase markers. To observe this rapid endocytosis, we have constructed a strain that secretes green fluorescent protein (GFP) from the muscle into the body cavity (*Pmyo-3::ssGFP*). In wild-type animals, the secreted GFP is rapidly endocytosed by the coelomocytes and degraded. In mutants for coelomocyte uptake (Cup mutants), GFP is not endocytosed but instead accumulates in the body cavity (see Figure 3A for mutant phenotype). In a screen for Cup mutants, we identified two alleles of the *cup-7* gene, *ar492* and *ar493*, which exhibited defects in coelomocyte uptake and were also uncoordinated (14). In this article, we demonstrate that *cup-7* encodes a PMCA previously named *mca-3*. In *mca-3* mutants, trafficking of fluid phase components to the lysosome is blocked in the early stages. This defect can be rescued by lowering extracellular calcium and thus is likely a consequence of intracellular calcium buildup. Other PMCAs are not expressed in the coelomocytes; thus, MCA-3 uniquely contributes to the function of these cells. This study demonstrates that mutations in a specific PMCA, MCA-3, disturbs a distinct biological pathway, clathrin-mediated endocytosis, in the scavenger cells of *C. elegans*.

Results

### cup-7 *encodes MCA-3, a plasma membrane* Ca^{2+}*-ATPase*

Conventional mapping and molecular characterization of the *cup-7* mutations demonstrated that they are alleles of the calcium ATPase *mca-3*. Three-point mapping determined that *ar492* is located on chromosome IV between *lin-1* and *unc-33* (14). Position in this interval was then determined by mapping the *ar492* mutation relative to single-nucleotide polymorphisms (SNPs) in a Hawaiian strain. SNP mapping narrowed the location of *ar492* to an interval between polymorphisms T23E1 and Y54G2A (IV: −5.94 and IV: −6.88) (Figure 1A). This interval contains 30 open reading frames (ORFs). One of them, *mca-3*, was reported to have an RNA interference phenotype resembling the uncoordinated phenotype of *ar492* (15,16) and therefore seemed a likely candidate. The *mca-3* gene was sequenced in the *ar492* and *ar493* strains, and lesions were identified in this gene in both strains (Figure 1B–D).

For clarity, this gene will be referred to as *mca-3* (membrane calcium ATPase) instead of *cup-7* for the remainder of the article. To determine the amino acid sequence of the protein, we analyzed the mRNAs from this locus using reverse transcriptase–polymerase chain reaction (PCR) (Figure 1B). The MCA-3 protein belongs to the family of PMCAs, molecular pumps that utilize the energy from ATP hydrolysis to extrude Ca^{2+} ions from the cytosol of the cell (17). There are three PMCAs encoded in the worm genome: MCA-1, MCA-2 and MCA-3 (17). Of the three, MCA-3 has the highest sequence identity (62%) to mammalian PMCAs (Figure 1E).

Based on sequence homology to mammalian PMCAs, we can infer the structure of MCA-3. MCA-3 consists of a short intracellular amino terminus, a total of 10 transmembrane domains, a cytosolic ATPase domain between transmembrane domains 4 and 5, and a cytosolic calmodulin-binding domain at the carboxyl terminus (Figure 1C). Our analysis of cDNAs revealed that *mca-3* has three splice variants, *a*, *b* and *c*, at its carboxyl terminus (Figure 1B). Alternative splicing at this location is conserved among most PMCAs and is proposed to affect binding affinity to calmodulin, thereby producing pumps with different Ca^{2+} sensitivities (18). MCA-3 isoforms *b* and *c* contain alternative calmodulin-binding domains. Isoform *a* resembles the splice pattern of isoform *c*; however, it also contains a short 69-bp exon that inserts 23 amino acids into the middle of the consensus calmodulin-binding site; this insertion could possibly render the pump insensitive to regulation by calmodulin. While overall sequence identity between MCA-3 and mammalian PMCAs is 62%, two regions reach over 90% identity. Both of these regions fall in the ATPase domain: one in the vicinity of the phosphorylation site within residues 410–435, and the other at the carboxyl-terminal end of the ATPase domain comprising residues 760–800.

The two mutant alleles are missense mutations in highly conserved residues and affect all three splice forms of *mca-3*. The PMCAs are highly similar to the sarcoendoplasmic reticulum calcium ATPases (SERCAs). Thus, we can speculate on the functions of mutated residues based on mutational analyses of the SERCAs (19). In *ar493*, a glycine (G786) is replaced by a glutamic acid in the ATPase domain (Figure 1C,D). In SERCAs, this glycine interacts with an aspartic acid residue through a van der Waals contact, which allows the aspartic acid to bind to Mg^{2+}. The Asp–Mg^{2+} in turn is necessary for conformational change of the pump (19). Based on sequence homology, the Gly786Glu mutation is likely to prevent Asp–Mg^{2+} binding and thus hinder a conformational change during the pump cycle. In *ar492*, a conserved asparagine (N954) is replaced by a lysine near the mouth of the pore in the extracellular loop between TM7 and TM8 (Figure 1C,D).

To confirm that mutations in *ar492* and *ar493* cause partial loss-of-function and not gain-of-function or neomorphic properties, we disrupted the *mca-3* locus using RNA
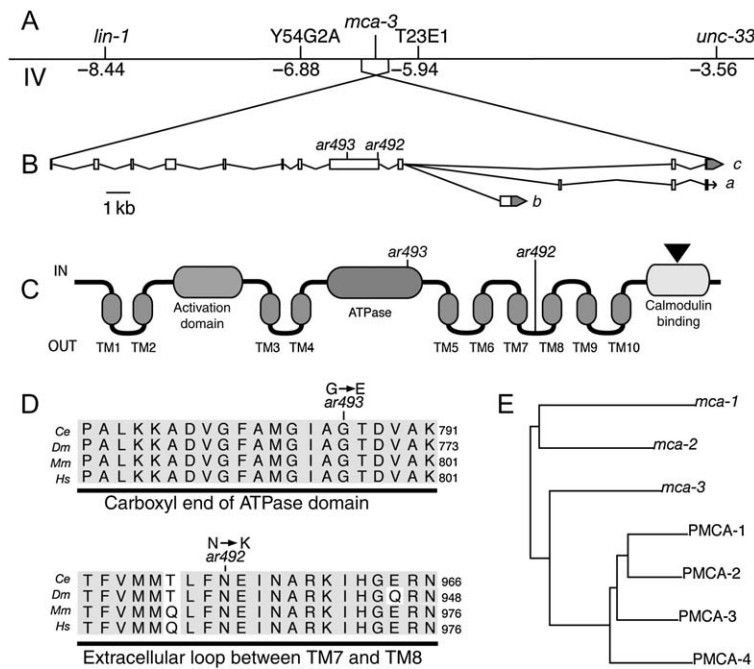
Figure 1: Gene structure of *mca-3*. A) *ar492* maps within a small interval on the left arm of chromosome IV. B) Exon and intron structure of *mca-3*. The 3′ end is differentially spliced to produce splice variants *a*, *b* and *c*. The mutations in *ar492* and *ar493* affect all three isoforms. C) MCA-3 predicted protein domains. Mutations present in *mca-3* alleles are indicated. Triangle indicates the location of the differential splice site. D) Sequence alignment of segments from *Caenorhabditis elegans* MCA-3 (*Ce*; accession #NP001023556), fly (*Ds*; accession #NP726565), mouse (*Mm*; accession #BAA83105) and human (*Hs*; accession #AAA36456) PMCAs. Missense mutations in *mca-3* alleles *ar492* and *ar493* are indicated above the alignments. E) Phylogenetic tree of the worm and human PMCAs. The bootstrap method with 'neighbor-joining' search was used to generate the tree. Alignments were performed using CLUSTALX and NJPLOT (Genetics Computer Group). MCA-3 is the closest homolog of mammalian PMCAs.

interference (RNAi). RNAi of *mca-3* in a wild-type background decreased coelomocyte staining in 36% of the animals ($n = 80$ animals). In addition, 45% of the RNAi adult animals were paralyzed, similar to the two mutant alleles. Only a subset of RNAi animals exhibited both the Cup defect and uncoordinated movement, which is consistent with partial penetrance of RNAi effects. *mca-3* RNAi also caused 8% (± 2.5) of the progeny to arrest as embryos, which is a phenotype that was not observed in the mutant strains. These data indicate that the *mca-3* mutations are loss-of-function alleles rather than gain-of-function mutations because they act in the same direction as RNA interference. They also suggest that *mca-3* loss-of-function phenotype is possibly lethal.

To better determine the null phenotype, we performed *mca-3* RNAi in the *ar492* and *ar493* backgrounds. This experiment produced a range of phenotypes that were more severe than observed for RNAi in the wild type: treated animals exhibited more embryonic lethality ($20.5 \pm 4.93\%$; $p < 0.005$ RNAi in *ar492* versus RNAi in wild type), larval arrest, slow growth, more severe paralysis and an onset of the Cup defect in larvae rather than in adults. These RNAi experiments confirm that *ar492* and *ar493* mutants reduce but do not eliminate protein function. They also indicate that a molecular null of *mca-3* is likely to cause embryonic lethality similar to the knockout mutations in the mouse.

### mca-3 *is expressed in the coelomocytes, nervous system, intestine and muscles*
There are three PMCA genes in the nematode. These three genes may contribute additively to calcium homeostasis of a cell; alternatively, each gene may be specialized for the

calcium dynamics of a particular tissue. We analyzed the temporal and spatial pattern of *mca* gene expression by placing GFP under the control of each of the upstream regulatory sequences. The *mca-1* GFP reporter is expressed only in one cell, the excretory canal (Figure 2A). For the *mca-2* promoter, GFP is only present in the epidermis (Figure 2B). We did not detect expression of the *mca-1* or *mca-2* reporters in the coelomocytes (Figure 2A,B).

Because of the specific defects observed in the mutants, we expected that *mca-3* would be expressed in the coelomocytes and the nervous system. The *mca-3* GFP reporter is transcribed from embryogenesis through adulthood in many tissues, including body muscle, the nervous system, the intestine and the coelomocytes (Figure 2C). We did not detect expression of the *mca-3* promoter in the epidermis or in the excretory canal, the tissues that express the other two *mca* genes. Although it is possible that these reporter constructs missed regulatory sequences, the data indicate that the worm PMCAs are expressed in complementary patterns. Thus, they are not likely to play redundant functions.

MCA-3 localizes to the plasma membrane and acts in a cell autonomous fashion
Based on high conservation between MCA-3 and mammalian PMCAs, we predicted that MCA-3 protein would act at the plasma membrane. To determine the subcellular localization of MCA-3, we generated tagged constructs expressing GFP-MCA-3 isoforms *a*, *b* and *c* under a coelomocyte-specific promoter. As expected, we found that all three isoforms of MCA-3 localize to the plasma membrane of coelomocytes (Figure 2D). Each of these constructs fully
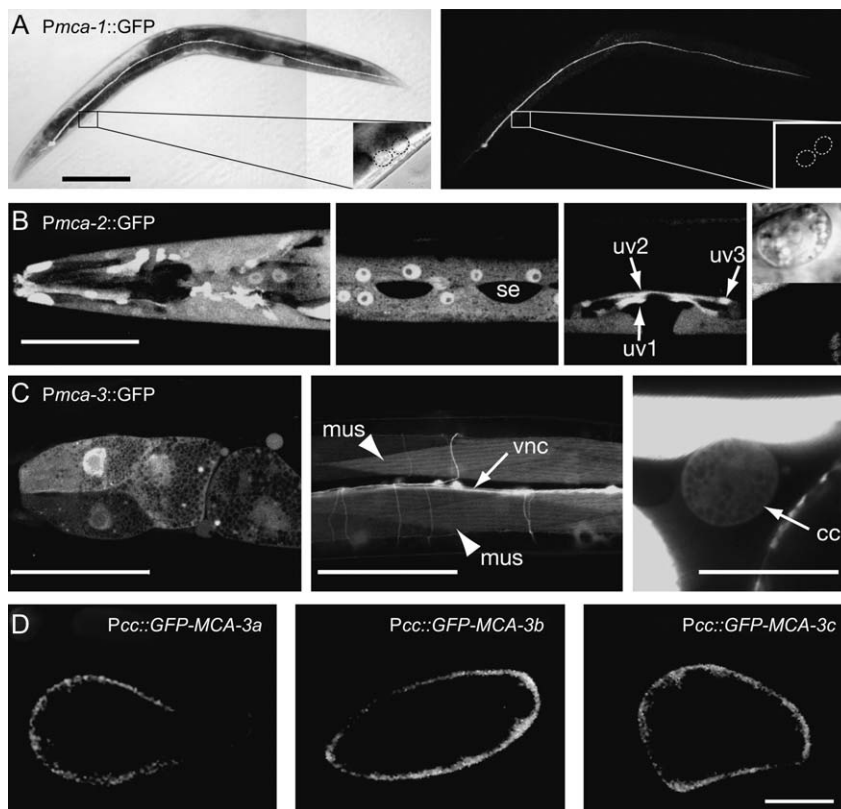
Figure 2: Expression pattern of the worm PMCAs and subcellular localization of MCA-3. A–C) Confocal micrographs of adult hermaphrodites expressing GFP under the *mca-1*, *mca-2* or *mca-3* promoters. A) *Pmca-1a* is expressed in the excretory canal. Low-magnification Nomarski (left) and fluorescent (right) images of *Pmca-1a*::GFP. Ventral is down, anterior left. Scale bar is 200 μm. Insets: high-magnification Nomarski (left) and fluorescence (right) images of coelomocytes. The coelomocytes are outlined with a dotted line and do not express *mca-1*. B) *Pmca-2* is expressed in epidermal tissues. High-magnification confocal images of *Pmca-2*::GFP. Left panel, head epidermis (including amphid sheath cells and amphid socket cells); middle left panel, syncytial cell hyp7, seam cells (se) do not express *mca-2*; the bright spots in the image are the nuclei of the multinucleated cell hyp7; middle right panel, vulval epithelial cells uv1, uv2 and uv3; right panel, Nomarski (top) and fluorescence (bottom) images of a coelomocyte which does not express *mca-2*. Scale bar (except for coelomocyte images) is 50 μm. C) *Pmca-3* is expressed in the nervous system, the intestine, the muscle and the coelomocytes. Anterior is left, ventral surface facing the viewer. Left panel: longitudinal section of anterior intestine. Middle panel: anterior ventral nerve cord; arrowhead indicates a muscle cell (mus), arrow points to the ventral nerve cord (vnc). Right panel: high-magnification picture of a coelomocyte (cc). Bright staining is the muscle (top) and the intestine (left). Scale bar: 50 μm in the left and middle panels and 20 μm in the right panel. D) Rescuing constructs of all three MCA-3 isoforms localize to the plasma membrane (*n* = at least 20 coelomocytes of each genotype). GFP was fused to cDNAs encoding the isoforms *a*, *b* and *c* and placed under the control of the coelomocyte promoter from the *unc-122* gene (see *Materials and Methods*). All three constructs rescued the *mca-3* mutant defect in coelomocyte endocytosis. Confocal images of an adult coelomocyte expressing the indicated MCA-3 isoforms fused to GFP at the amino terminus are shown. Bar is 5 μm.

rescued the endocytosis defect of *mca-3(ar492)* mutant worms indicating that the protein fusions are functional and that MCA-3 acts cell autonomously in regulating endocytosis of the coelomocyte (Figure 3A,B). As expected, these constructs did not rescue the uncoordinated defect of this mutant strain because the promoter used for these constructs is not expressed in the nervous system.

MCA-3 is required during endocytosis
Previous experiments indicate that loss of PMCA function is often associated with apoptotic cell death (4–8). To determine whether *mca-3* mutations affect the viability of coelomocytes, we counted the coelomocytes in *mca-3* mutants. We examined two strains that express GFP in

the coelomocytes of *mca-3(ar492)* animals (10 animals each). In both strains, there are a wild-type number of these cells—six per animal—suggesting that the defect in GFP uptake is not because of cell death but rather a defect in endocytosis in these scavenger cells.

The coelomocyte uptake defect in mutants suggested that MCA-3 was required for endocytosis in the coelomocytes. To determine the particular step of endocytosis affected in the *mca-3* animals, we examined GFP distribution in the mutants. In wild-type worms, GFP is taken up by coelomocytes into endosomes and then is targeted to lysosomes for degradation (20). Cup mutants fall into two groups: mutations in the first group affect either early
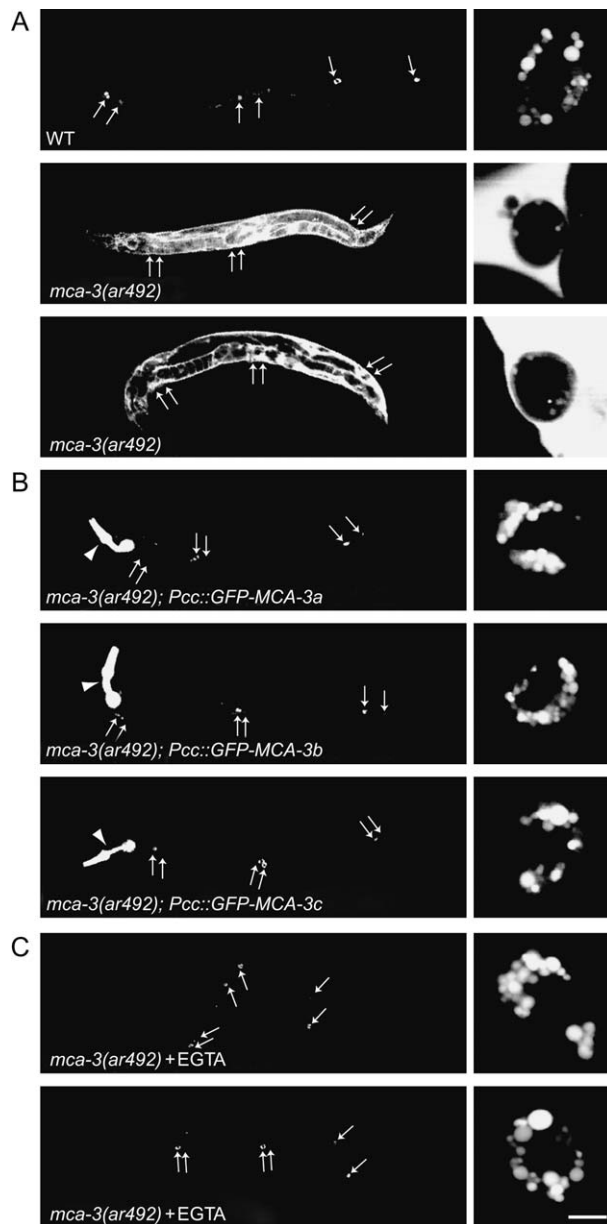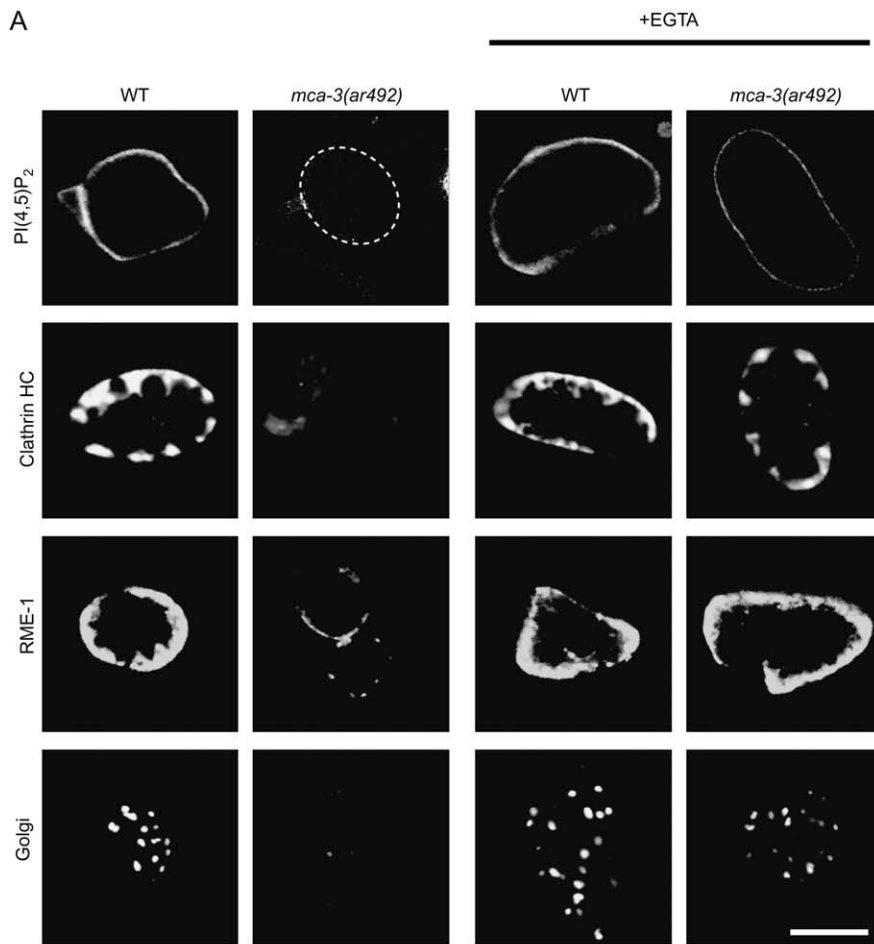
Figure 3: MCA-3 is required for endocytosis in coelomocytes.
A–C) Confocal images of adult hermaphrodites secreting GFP from the muscles into the body cavity (*arIs37*, *n* = at least 80 animals of each genotype). The left column shows whole worms at a low magnification. Arrows indicate the positions of the coelomocytes in the worms; not all six coelomocytes are evident in each section. Genotypes of the imaged animals are indicated. In the wild type, the shape of the body is not visible because GFP fluorescence is confined to the six scavenger cells. In *mca-3* mutants, the body cavity fills with GFP in the extracellular space and the shape of the animal is visible. The right column shows individual coelomocytes at a higher magnification from these animals. Coelomocytes are large solitary scavenger cells; the bright spots are GFP-loaded vesicles within a single coelomocyte. In *mca-3* mutants, the coelomocyte appears as a dark cell surrounded by GFP in the extracellular space. Bar is 5 μm in higher magnification images. A) Mutations of *mca-3* result in a Cup phenotype in adult animals. In wild-type animals, coelomocytes clear the GFP from the body cavity, whereas in both *mca-3* mutant strains GFP accumulates in the body cavity. B) Coelomocyte-specific expression of each MCA-3 isoform is sufficient to rescue the Cup defect. Images of *mca-3 (ar492)* mutant animals expressing the indicated *mca-3* isoforms under a coelomocyte-specific promoter. Arrowheads indicate GFP expressed in the pharynx, which was used as a transgenic marker. '*Pcc*'indicates the coelomocyte-specific promoter of the *unc-122* gene (see *Materials and Methods*). C) Growth in limiting calcium conditions rescues the Cup defect. Images of *mca-3* mutant animals grown on plates containing 1 mM EGTA.

number and sizes of GFP-filled vesicles in the coelomocytes (Figure 3A, right column).
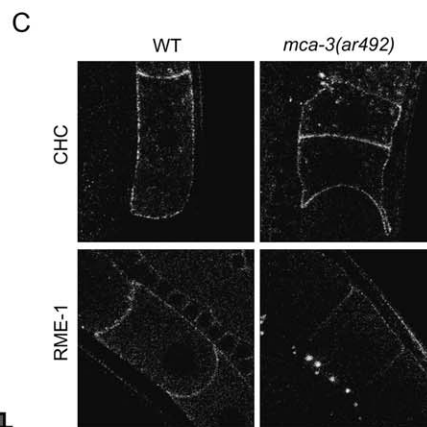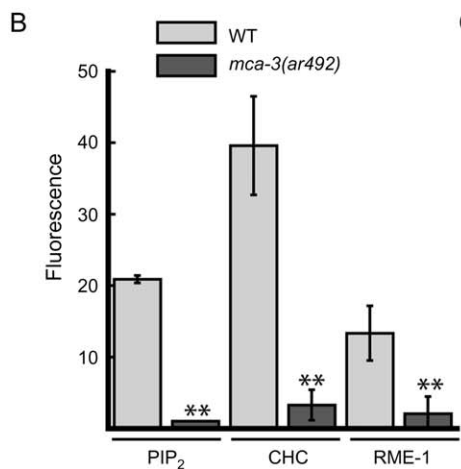
The early steps of endocytosis consist of the following events. First, the machinery for endocytosis is recruited to the endocytic site. Second, the clathrin coat assembles and the membrane invaginates to form a coated pit. Third, the deeply invaginated pit is separated from the membrane by the GTPase dynamin. Finally, the clathrin coat is removed from the nascent vesicle. To determine which step of endocytosis is affected in *mca-3* mutants, we examined the localization of different molecular markers of endocytosis. To assay recruitment of the endocytic machinery to the plasma membrane, we determined the distribution of clathrin heavy chain (22), of RME-1, an EH domain-containing protein required for endocytosis (14,21), and of phosphatidylinositol-4,5-bisphosphate $(PI(4,5)P_2)$. We assayed $PI(4,5)P_2$ by the localization of the pleckstrin homology domain of mouse phospholipase C δ fused to GFP (PH::GFP) (23). In the wild type, $PI(4,5)P_2$ causes PH::GFP to be localized to the plasma membrane (Figure 4A,B). In the *mca-3* mutants, PH::GFP fluorescence at the plasma membrane was severely reduced, and we conclude that $PI(4,5)P_2$ levels were reduced. $PI(4,5)P_2$ is likely to be important for endocytosis because it recruits the adaptor complexes AP2 and AP180 to the plasma membrane, which then recruit clathrin (24,25). As predicted, given the low levels of $PI(4,5)P_2$ in *mca-3* mutants, the localization of clathrin heavy chain to the plasma membrane was severely reduced (Figure 4A,B). In wild-type coelomocytes, RME-1 localizes to the internal vesicles and to the plasma

steps in endocytosis or endosomal recycling, and result in an almost complete block of uptake of the secreted GFP (14). This group includes mutants deficient in clathrin, dynamin and RME-1, an EH domain protein required for endosomal recycling (14,21). The second group comprises genes participating in trafficking from the endosome to the lysosome. In this latter class, GFP is still cleared from the body cavity but it is not degraded and instead accumulates in large vesicles within coelomocytes (20). In *mca-3* mutants, GFP does not accumulate in the coelomocytes but rather accumulates in the body cavity (Figure 3A, left column), and thus these mutations block early steps in endocytosis. The uptake defect is first visible in L4 larvae or young adults. At this point, GFP starts to accumulate in the body cavity and there is a severe reduction in the

A

B

C

Figure 4: MCA-3 is required for plasma membrane localization of endocytic markers in coelomocytes. A) Plasma membrane and Golgi markers show abnormal staining in *mca-3*-deficient coelomocytes, which can be rescued by growth in limiting calcium conditions. Confocal micrographs of coelomocytes in wild-type and *mca-3(ar492)* adult hermaphrodites raised on normal or EGTA-containing plates. Background genotype and growth conditions are indicated at top. Animals in different rows express the following GFP fusion proteins (from top to bottom): PLC delta-PH domain (array *cdIs80*) to monitor PI(4,5)P$_2$, clathrin heavy chain (array *bIs5*), an EH hand protein RME-1 (array *cdEx39*) and a Golgi marker mannosidase II (array *cdIs54*). Bar is 5 μm in all images. Images of wild-type and mutant coelomocytes were taken with the same exposure and magnification for each marker. In the image of the PLC delta-PH domain-GFP in *mca-3* mutant, the coelomocyte is outlined. B) Plasma membrane-associated endocytic markers have decreased levels in *mca-3(ar492)* mutants. Quantification of fluorescence of the indicated markers in wild-type and mutant coelomocytes. **p < 0.05, error bars represent standard deviation. C) Endocytic markers are not mislocalized in oocytes of *mca-3* mutant animals. Confocal micrographs of oocytes in wild-type and *mca-3(ar492)* mutant animals expressing GFP fusions to the indicated proteins. Bar is 10 μm in all images.

membrane (21), and retrieves endocytosed receptors from the sorting endosome to the plasma membrane (21,26). Previous studies indicated that this localization pattern is perturbed in endocytic mutants such as *cup-4* (27). In *mca-3* mutants, RME-1 fluorescence is reduced to 16% of wild-type level in the coelomocytes (Figure 4C). It is possible that the depletion in RME-1 is caused by the depletion in clathrin because the RME-1 homolog EHD1 binds clathrin

(28). However, it is also possible that the reduction of RME-1 occurs because of a buildup of intracellular calcium. These results indicate that MCA-3 is required for the first step of endocytosis: the recruitment of the endocytic machinery to the plasma membrane.

Markers for later compartments such as endosomes and lysosomes were not mislocalized indicating that late

trafficking steps are unaffected (Figure 5). However, these compartments were reduced in size and the endoplasmic reticulum (ER) (29) was dispersed in *mca-3* mutants (Figure 5). The decrease in the size of endosomes and lysosomes and the dispersal of the ER are common to all *cup* mutants that block endocytosis and are likely to be an indirect consequence of the defect in uptake and reduction in trafficking in these mutants (27). *mca-3* mutations also resulted in what appeared to be smaller Golgi stacks as visualized by mannosidase II-GFP (Figure 4A) (20). This
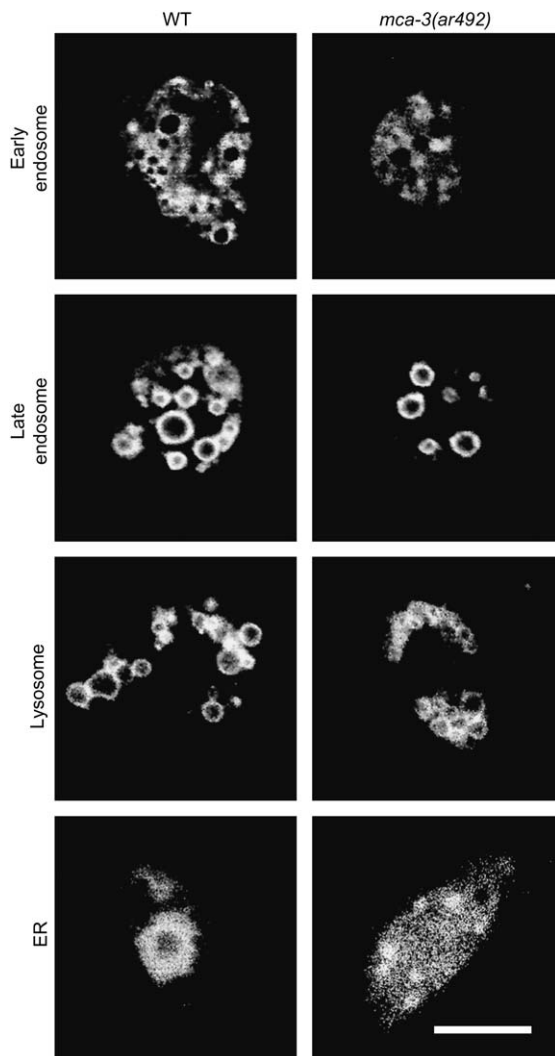
| | WT | *mca-3(ar492)* |

Figure 5: *mca-3* mutations do not disrupt the trafficking from endosomes to lysosomes. Confocal micrographs of coelomocytes in wild-type and *mca-3(ar492)* adult hermaphrodites expressing GFP fusions to RAB-5 (early endosome), RME-8 (late endosome), CUP-5 (lysosome) and cytochrome b5 (ER). Distributions of markers for the endosome to lysosome pathway are similar to those of the wild type. By contrast, the ER is dispersed in *mca-3(ar492)* instead of being perinuclear. Images of wild-type and mutant coelomocytes were taken with the same exposure and magnification. Bar is 5 μm in all images.

defect is likely as a result of high cellular calcium because increased calcium levels cause a similar phenotype in yeast cells (30).

Another tissue with high rates of endocytosis is the gonad. Yolk is secreted by the gut, and endocytosed by the developing oocytes in a clathrin-mediated process (31). To determine if calcium clearance by MCA-3 was important for endocytosis in oocytes, we examined uptake of GFP-tagged vitellogenin. In contrast to our previous observations (14), MCA-3 does not seem to be required for endocytosis in the germ line. Vitellogenin was not mislocalized in *mca-3(ar492)* or in *mca-3(RNAi)* animals (data not shown). In addition, clathrin and RME-1 were not mislocalized in the oocytes of *mca-3* mutants (Figure 4C). These results indicate that MCA-3 is not required for endocytosis by oocytes.

Coelomocyte uptake can be rescued by limiting extracellular calcium

Because MCA-3 is responsible for clearance of calcium from the cytosol, then mutations in *mca-3* are likely to cause an increase in internal calcium. To test whether calcium buildup is responsible for the observed *mca-3* mutant phenotype, we lowered the extracellular calcium levels by growing animals on plates containing 1 mM EGTA. EGTA rescued GFP uptake into coelomocytes in *mca-3* mutants (Figure 3C), restored $PI(4,5)P_2$ levels and localized the early endocytic proteins to the plasma membrane (Figure 4A). This result is consistent with the hypothesis that the endocytic block in *mca-3* mutants is caused by inappropriate calcium clearance because of the mutated calcium pump (also see *Discussion*).

Discussion

Ca^{2+} homeostasis is required to maintain proper Ca^{2+} signaling and cell survival. Plasma membrane calcium ATPases, along with NCXs, are responsible for expulsion of calcium from the cytosol into the extracellular space. Here we present evidence that under physiological conditions, a worm PMCA encoded by the *mca-3* gene is an important regulator of endocytosis. Our results indicate that the MCA-3 protein acts in the initial steps of endocytosis, likely during the recruitment of the endocytic machinery to the membrane. First, as expected, MCA-3 localizes to the plasma membrane, the site of endocytosis. Second, the *mca-3* mutant phenotype mimics the phenotypes of other early endocytic mutants such as clathrin or dynamin. Third, *mca-3* mutations cause mislocalization of the plasma membrane-localized components of endocytosis, the proteins clathrin and RME-1 as well as reduction of the lipid $PI(4,5)P_2$. Fourth, analysis of the remaining PMCAs indicates that MCA-3 is a non-redundant regulator of endocytosis. Finally, the *mca-3*-associated endocytic defect can be rescued by growing animals under limiting calcium

conditions. In the following paragraphs, we will discuss three questions: (1) Are defects present in *mca-3* mutants because of excess calcium? (2) Are calcium ATPases specifically devoted to particular cell biological processes? (3) How could excess calcium inhibit endocytosis?

Are defects present in *mca-3* mutants due to excess calcium? Because PMCAs pump calcium out of cells in biophysical reconstitution experiments (32), it is expected that calcium secretion is their main activity in the cell. Indeed, several studies demonstrated that PMCAs play a role in calcium secretion under physiological conditions and that calcium actually increases in cells with defective PMCA function. For example, pharmacological inhibition of PMCAs in neurons, smooth muscles and endothelial cells results in increased calcium levels (33,34). Consistent with these studies, we find that the cellular defects observed in worm PMCA mutants can be accounted for by aberrant calcium homeostasis. Specifically, reducing extracellular calcium rescued the mutant phenotype. Thus, while pharmacological experiments concluded that inhibition of PMCAs leads to intracellular calcium buildup, mutant studies can identify the functional consequences of calcium buildup.

Are calcium ATPases specifically devoted to particular cell biological processes? Our data indicate that partial loss of MCA-3 function causes inhibition of a specific cellular process, clathrin-mediated endocytosis. Similarly, loss of the brain-enriched PMCA2 leads to specific neurological defects such as deafness and balance problems, which are not necessarily related to cell death (6). These mutant mice are deaf, likely because of defects in the electrical gradient required for hair cell function (35–38). In addition, PMCA2 mutants lack the calcium carbonate accretions, called otoconia, that sense acceleration (35), and have reduced calcium levels in milk (39). These data suggest that PMCA2 functions in specific cell processes to tune calcium levels rather than just for anti-apoptotic functions. Cell- and tissue-specific expression patterns of different genes and splice forms also suggest that PMCAs are committed to the regulation of individual biological processes. Our data are consistent with these findings: MCA-3 may be responsible for fine-tuning calcium levels for efficient clathrin-mediated endocytosis.

Although it is tempting to imagine that the PMCAs are exclusively dedicated to specific processes, such as endocytosis, it should be recognized that the PMCA expression may affect any process sensitive to calcium. Although endocytosis may be particularly sensitive to loss of PMCAs, the defects in *mca-3* mutant animals are not limited to endocytosis. For example, both alleles of *mca-3* cause abnormalities in Golgi structures, a phenotype previously reported in yeast cells in response to abnormal changes in calcium levels (30).

How does excess calcium inhibit endocytosis? Most of the work on the role of calcium in endocytosis comes from the studies of synaptic vesicle recycling at nerve terminals. At synapses, calcium influx is necessary to activate endocytosis (40). Similarly, in non-neuronal cells some studies indicate that calcium is required for endocytosis (41,42). By contrast, our results demonstrate that elevated calcium levels inhibit endocytosis. An inhibitory role for calcium in endocytosis was originally proposed by von Gersdorff and Matthews (43). In these experiments, calcium influx induced by ionomycin inhibited synaptic vesicle endocytosis. In non-neuronal cells, high calcium was found to inhibit fluid phase endocytosis in epidermoid cells and receptor endocytosis of EGF in pancreatic cells and fibroblasts (44,45). One possible target of high calcium is dynamin because Robinson and Cousin reported that high concentrations of calcium could inhibit dynamin in *in vitro* assays (46). Another possibility is that the observed inhibition of endocytosis results from low levels of plasma membrane $PI(4,5)P_2$. $PI(4,5)P_2$ is required for nucleation of endocytosis because it provides a membrane anchor for the clathrin adaptor complexes AP2 and AP180 (24,25). Thus, absence of $PI(4,5)P_2$ would likely result in mislocalization of clathrin and an overall inhibition of endocytosis. Reduction of $PI(4,5)P_2$ could also affect localization of other endocytic components; for example, both dynamin and epsin are recruited to the plasma membrane by binding $PI(4,5)P_2$ via their phospholipid-binding domains (47). How does loss of *mca-3* function reduce phosphoinositide levels? One possibility is that $PI(4,5)P_2$ is metabolized by phospholipase C. Indeed, phospholipase C δ can be directly activated by calcium (48), and activation of this enzyme has been demonstrated to inhibit clathrin-mediated endocytosis of apical proteins in renal epithelial cells (49). To assess whether *mca-3* acts through hyperactivation of a *plc* gene, we perturbed all five worm phospholipase C (PLC) genes by RNAi. Although the known phenotypes for these knockdowns were observed, endocytosis in the coelomocytes was not rescued (data not shown). Thus, it is likely that the *mca-3* endocytosis defect is only partially due to reduction in $PI(4,5)P_2$ levels and increased calcium is affecting multiple proteins required for endocytosis. It is also possible that calcium buildup has an indirect effect on endocytosis. While we have not observed any indications of apoptosis in either of the *mca-3* mutants, increased calcium levels could well affect the overall cell health and simply slow down any processes occurring within the cell. Finally, calcium influx is used as a second messenger in the cell; thus, aberrant calcium clearance could influence other biological processes that could in turn inhibit endocytosis. While the specific molecular targets of high calcium still need to be identified, our data and other work suggest that a buildup of calcium inhibits endocytosis. This hypothesis is especially interesting because most studies indicate that calcium also plays a role in activation of endocytosis. It is thus likely that at least in coelomocytes the response of endocytosis to intracellular calcium is bipartite: the initial rise of calcium activates endocytosis, but prolonged high levels of calcium inhibit the same process.

Materials and Methods

Strains

Wild-type strains were *C. elegans* isolates from Bristol (strain N2). Mapping experiments used the polymorphic strain from Hawaii CB4856. GFP secretion strain GS1912 *dpy-20(e1282) arIs37[Pmyo-3::ssGFP]* IV was used in screens for coelomocyte uptake. Two isolated *mca-3* mutant strains were GS2526 *mca-3(ar492) dpy-20(e1282) arIs37[Pmyo-3::ssGFP]* IV and GS2527 *mca-3(ar493) dpy-20(e1282) arIs37[Pmyo-3::ssGFP]* IV. *mca-3* expression analysis was performed using strain EG3350 *oxEx593[Pmca-3::GFP]*. Sub-cellular localization and rescue experiments used strains NP877 *unc-119 (ed3)* III; *cdIs72[Pcc::GFP-MCA-3a, Pmyo-2::GFP, unc-119⁺]*, NP877 *unc-119(ed3)* III; *cdIs63 [Pcc::GFP-MCA-3b, Pmyo-2::GFP, unc-119⁺]* and NP894 *unc-119(ed3)* III; *cdIs70[Pcc::GFP-MCA-3c, Pmyo-2::GFP, unc-119⁺]*. Yolk uptake was analyzed using strain DH1006 *bIs1[vit2::GFP, rol-6 (su1006)]*. For analysis of markers, the following strains were used: clathrin heavy chain-GFP strains DH1116 *bIs5[CHC::GFP, rol-6(su1006)]* and NP958 *mca-3(ar492); bIs5[CHC::GFP, rol-6(su1006)]*, PLC delta-PH domain-GFP strains NP898 *cdIs80[Pcc1::PLCd::GFP, rol-6(su1006)]* and *NP927 mca-3 (ar492); cdIs80[Pcc1::PLCd::GFP, rol-6(su1006)]*, RME-1-GFP strains NP187 *cdEx39[Pcc1::GFP::RME-1(271a1), Pmyo-2::GFP]* and NP661 *mca-3 (ar492); cdEx39[Pcc1::GFP::RME-1(271a1), Pmyo-2::GFP]*, RAB-5-GFP strains NP212 *cdEx49[Pcc1::GFP::RAB-5, Pmyo-2::GFP]* and NP715 *mca-3 (ar492); cdEx49[Pcc1::GFP::RAB-5, Pmyo-2::GFP]*, RME-8-GFP strains DH1336 *bIs34[rme-8-GFP, rol-6(su1006)]* and NP654 *mca-3s(ar492); bIs34[rme-8-GFP, rol-6(su1006)]*, CUP-5-GFP strains NP249 *cdEx60[Pcc1::GFP::CUP-5, rol-6(su1006)]* and NP640 *mca-3(ar492); cdEx60[Pcc1::GFP-CUP-5, rol-6(su1006)]*, cytochrome b5-GFP strains NP738 *unc-119(ed3); cdIs36[pcc1::C31E10.7-GFP, unc-119(+), Pmyo-2 ::GFP]* and NP810 *mca-3(ar492); cdIs36[pccl::C31E10.7-GFP, unc-119(+), Pmyo-2::GFP]*, and mannosidase II-GFP strains NP822 *unc-119(ed3); cdIs54[pcc1::MANS-GFP, unc-119(+), Pmyo-2::GFP]* and NP860 *mca-3 (ar492); cdIs54[pcc1::MANS-GFP, unc-119(+), Pmyo-2::GFP]*. Expression of *mca-2* was analyzed using strain EG3992 *oxEx732[Pmca-2::GFP]*.

Mapping

Previous mapping determined that *ar492* is located on chromosome IV between *lin-1* and *unc-33* (14). Fine mapping was performed using single nucleotide polymorphisms (SNPs) (50). Briefly, 96 F2 Cup progeny were isolated from *ar492*/Hawaiian heterozygotes. PCR revealed that 1/96 Cup progeny were heterozygous for a Hawaiian polymorphism close and on the left side at −6.88 (Y54G2A.22) and 1/96 was close and on the right side at −5.94 (T23E1.1) (Figure 1A). Based on RNA interference phenotype, only one gene, *mca-3*, was a good candidate (15,16). Both alleles *ar492* and *ar493* were sequenced at the *mca-3* locus at the University of Utah sequencing facility, and were confirmed to have molecular lesions in the *mca-3* ORF (Figure 1C). The ethane methyl sulphonate (EMS)-induced lesions result in the following missense mutations: in *ar492* asparagine 954 is mutated to a lysine (transversion aat to aaG), and in *ar493* glycine 786 is mutated to a glutamic acid (transition gga to gAa).

cDNA analysis

Wild-type cDNA was generated by reverse transcription of total RNA extracted from 10 small plates of wild-type worms. Worms were lysed in 1 mL Trizol reagent (Gibco-BRL/Invitrogen, Carlsbad, CA, USA), and cellular debris was removed by centrifugation. RNA was purified by isopropanol and ethanol precipitations and resuspended in water. Two-hundred and fifty nanograms of RNA was used for each reverse transcription reaction using SuperScriptTM II RT (Invitrogen). The common exons were amplified in two PCR reactions; the C-terminal splice variants were obtained in separate PCR reactions. For first DNA strand synthesis of common exons, the 5′ portion was generated using primer oEB242 [GCTGCAGCGACAGCTTTTC] and 3′ portion was generated with oEB246 [GTTAACCCACGGACCCAAA-GAAT]. The DNA was then amplified with PCR using primers pairs oEB242/ oEB241 [GTGCTAGCCTGGAGGAGCTTC] (5′ region of common exons) and oEB243 [GCACAGGCGCTTCTCGAC]/oEB244 [CATATTTGTCAGATGGCT-GAGC] (3′ region of common exons), and cloned into a TA cloning vector

pCR2.1 (Invitrogen) to yield plasmids p3 and pE, respectively. Primer oEB241 appends a 5′ NheI site on the 5′ end of the DNA that was later used to generate expression constructs. C-terminal differential splicing predicted by WORMBASE [http://www.wormbase.org, release WS110, 1 October, 2003] was confirmed as follows. Primers oEB249 [CTATA-GATTGTTCGTCTCCTTGATA] and oEB248 [TTACACGTGAGCAACA-GAAACTG] were designed to anneal to the very 3′ end of isoforms *a* and *c* (oEB249) and isoform *b* (oEB248), and used to generate the first DNA strand. The termini were then amplified by PCR using those primers and a 5′ primer oEB245 [CACAGGAGAAGCTCGACTTG], TA cloned to yield plasmids p3end-a (isoform *a*), p3end-b (isoform *b*) and p3end-c (isoform *c*). High fidelity PCR was performed using pHusion (Finnzymes, Espoo, Finland); all plasmids were sequenced to confirm wild-type sequence.

Inhibition via RNA interference

5′ (922 bp) coding region from the 5′ region of *mca-3* was PCR amplified using oligos 5′GTGCTAGCCTGGAGGAGCTTC and 5′GCTGCAGCGACAG-CTTTTC and cloned into pCR-Blunt (Invitrogen). Inserts in both orientations were used as templates for T7 *in vitro* transcription (Riboprobe Combination System T3/T7, Promega, Madison, WI, USA). Sense and antisense strands were mixed together at 0.1 mg/mL, annealed (65°C for 1 min, 50°C for 5 min, slow ramp to 20°C over 5 min), and injected into 10 wild-type young adults. Progeny of injected animals were analyzed for defects in GFP uptake by the coelomocyte as well as general locomotory defects.

GFP constructs

pEB73 (*Pmca-3*::GFP transcriptional fusion)

For expression analysis, a 2.5-kb region upstream of *mca-3* ATG was amplified from genomic wild-type DNA with oligos oEB232 [AATTCTGCAG-CACAATGGCTACAGTAGCC] and oEB237 [TTCTACCGGTACCCGAAGCTC-CTCCAGTGATG]. These primers append *Pst*I and *Age*I restriction sites, respectively. The promoter fragment was then inserted into a *Pst*I and *Age*I-digested Fire lab vector pPD95.75 to produce a transcriptional GFP fusion. The construct was injected into gonads of adult animals at concentration of 10 ng/μL, along with 90 ng/μL worm genomic DNA. Ten independent transgenic lines were generated and analyzed for GFP expression. All lines expressed GFP in the same tissues and one representative line *oxEx593* was analyzed using confocal microscopy.

Pmca-1::GFP transcriptional fusion

For expression analysis, a 3.4-kb region upstream of *mca-1* ATG was amplified from genomic wild-type DNA with oligos oEB340 [GAATGCATGCATGTTCA-GAAGACTGGGAAGG] and oEB341 [TCCTACCGGTCCTGCGTTAGTATCAG-GAGAGG]. These primers append *Sph*I and *Age*I restriction sites, respectively. The promoter fragment was then inserted into a *Sph*I and *Age*I-digested Fire lab vector pPD117.01 to produce a transcriptional GFP fusion. The construct was injected into gonads of adult animals at concentration of 10 ng/μL, along with 90 ng/μL worm genomic DNA. Twenty independent transgenic animals were generated and analyzed for GFP expression. All animals expressed GFP in the same tissue and were analyzed using confocal microscopy.

Pmca-2::GFP transcriptional fusion

For expression analysis, a 3.3-kb region upstream of *mca-2* ATG was amplified from genomic wild-type DNA with oligos oEB342 [GAATGCATG-CGTGCATTAATTTAGTTAGCATATACTG] and oEB343 [TTCTACCGGTCCG-CGGAGCTCCATGAGGAG]. These primers append *Sph*I and *Age*I restriction sites, respectively. The promoter fragment was then inserted into an *Sph*I-and *Age*I-digested Fire lab vector pPD117.01 to produce a transcriptional GFP fusion. The construct was injected into gonads of adult animals at concentration of ng/μL, along with 90 ng/μL genomic worm DNA. Three independent transgenic lines were generated and analyzed for GFP expression. All lines expressed GFP in the same tissues and one representative line *oxEx732* was analyzed using confocal microscopy.

Coelomocyte rescue constructs

cDNA fragments from p3 and pE were ligated together to produce a cDNA including the common exons in the 5′ region of the *mca-3* gene. This cDNA

was cloned into 3′ end constructs p3end-a, p3end-b and p3end-c to yield full-length cDNAs of each *mca-3* isoform. To analyze the subcellular localization of MCA-3, a fusion protein was constructed and put under the control of coelomocyte-specific promoter of *unc-122* (51). The minimal coelomocyte promoter and GFP were PCR amplified from the plasmid pPD97/98 (52) using primers oEB323 [GCATGCCCACGGAAATGACTATCAG] and oEB251 [GCTAGCACCATATTCTTTGTATAGTTCATCCATGCCATG]. These primers append 5′ SphI and 3′ NheI restriction sites that were used to insert the coelomocyte promoter and GFP into plasmid pPD117.01 (Fire lab vector). The *mca-3* full-length cDNAs were then cloned using the *Nhe*I site appended at the 5′ end of each *mca-3* isoform and *Eco*RV site present in the TA cloning vector pCR2.1 (Invitrogen) to yield plasmids Pcc::GFP-MCA3a (isoform *a*), Pcc::GFP-MCA3b (isoform *b*) and Pcc::GFP-MCA3c (isoform *c*). These plasmids were then gene gunned to generate arrays *cdIs72* (isoform *a*), *cdIs63* (isoform *b*) and *cdIs70* (isoform *c*), and analyzed for localization of the fusion protein. All N-terminal fusions showed plasma membrane localization and rescued the Cup phenotype. Lines expressing the rescuing constructs were further analyzed by confocal microscopy. In addition, we generated constructs with GFP fused to the C-terminus rather than the N-terminus of MCA-3. However, they accumulated in the cytoplasm and did not rescue the Cup defect, and therefore were deemed not functional (data not shown).

Analysis of markers for various compartments

Marker strains used are described in the earlier section of *Materials and Methods*. Coelomocyte counts were performed in NP654 *mca-3(ar492); bIs34[rme-8-GFP, rol-6(su1006)]* and NP860 *mca-3(ar492); cdIs54[pcc1:: MANS-GFP, unc-119(+), Pmyo-2::GFP]*. For analysis of protein distribution in *mca-3* mutants, coelomocytes were identified using Nomarski optics, confocal images of wild-type and *mca-3* mutant coelomocytes expressing GFP-fused markers were taken using a × 100 objective. Strains expressing the same marker were imaged with identical settings.

Analysis of fluorescence levels

Unaltered collected images were opened through IMAGEJ. The coelomocytes were selected with freehand and measured for average pixel intensity. For each genotype, three independent images were analyzed.

Growth on EGTA plates

To assay limiting calcium conditions, animals were grown on nematode growth medium (NGM) plates without calcium and with 1 mM EGTA.

Confocal microscopy

To analyze the tissue distribution of *mca* gene expression, animals carrying the GFP transcriptional constructs were immobilized using 50 mM sodium azide and imaged on a Pascal LSM5 confocal microscope using a Zeiss × 63 1.4 NA objective. For the remaining images, adult hermaphrodites were paralyzed in 10 mM levamisole, and the images were taken with a Nikon PCM 2000, using argon 488 excitation.

References

1. Macleod GT, Hegstrom-Wojtowicz M, Charlton MP, Atwood HL. Fast calcium signals in *Drosophila* motor neuron terminals. J Neurophysiol 2002;88:2659–2663.

2. Berridge MJ, Bootman MD, Roderick HL. Calcium signalling: dynamics, homeostasis and remodelling. Nat Rev Mol Cell Biol 2003; 4:517–529.

3. Orrenius S, Zhivotovsky B, Nicotera P. Regulation of cell death: the calcium-apoptosis link. Nat Rev Mol Cell Biol 2003;4:552–565.

4. Prasad V, Okunade GW, Miller ML, Shull GE. Phenotypes of SERCA and PMCA knockout mice. Biochem Biophys Res Commun. 2004; 322:1192–1203.

5. Shull GE. Gene knockout studies of Ca^{2+}-transporting ATPases. Eur J Biochem. 2000;267:5284–5290.

6. Okunade GW, Miller ML, Pyne GJ, Sutliff RL, O'Connor KT, Neumann JC, Andringa A, Miller DA, Prasad V, Doetschman T, Paul RJ, Shull GE. Targeted ablation of plasma membrane Ca^{2+}-ATPase isoforms 1 and 4 indicates a major housekeeping function for PMCA1 and a critical role in hyperactivated sperm motility and male fertility for PMCA4. J Biol Chem 2004;279:33742–33750.

7. Kurnellas MP, Nicot A, Shull GE, Elkabes S. Plasma membrane calcium ATPase deficiency causes neuronal pathology in the spinal cord: a potential mechanism for neurodegeneration in multiple sclerosis and spinal cord injury. FASEB J 2005;19:298–300.

8. Paszty K, Verma AK, Padanyi R, Filoteo AG, Penniston JT, Enyedi A. Plasma membrane Ca^{2+} ATPase isoform 4b is cleaved and activated by caspase-3 during the early phase of apoptosis. J Biol Chem 2002; 277:6822–6829.

9. Montell C. The latest waves in calcium signaling. Cell 2005;122:157–163.

10. Schuh K, Cartwright EJ, Jankevics E, Bundschu K, Liebermann J, Williams JC, Armesilla AL, Emerson M, Oceandy D, Knobeloch KP, Neyzes L. Plasma membrane Ca^{2+} ATPase 4 is required for sperm motility and male fertility. J Biol Chem 2004;279:28220–28226.

11. Liu L, Ishida Y, Okunade G, Shull GE, Paul RJ. Role of plasma membrane Ca^{2+}-ATPase in contraction-relaxation processes of the bladder: evidence from PMCA gene-ablated mice. Am J Physiol Cell Physiol. 2006;290:C1239–C1247.

12. Lumpkin EA, Hudspeth AJ. Regulation of free Ca^{2+} concentration in hair-cell stereocilia. J Neurosci 1998;18:6300–6318.

13. Dumont RA, Lins U, Filoteo AG, Penniston JT, Kachar B, Gillespie PG. Plasma membrane Ca^{2+}-ATPase isoform 2a is the PMCA of hair bundles. J Neurosci 2001;21:5066–5078.

14. Fares H, Greenwald I. Genetic analysis of endocytosis in *Caenorhabditis elegans*: coelomocyte uptake defective mutants. Genetics 2001; 159:133–145.

15. Kamath RS, Fraser AG, Dong Y, Poulin G, Durbin R, Gotta M, Kanapin A, Le Bot N, Moreno S, Sohrmann M, Welchman DP, Zipperlen P, Ahringer J. Systematic functional analysis of the *Caenorhabditis elegans* genome using RNAi. Nature 2003;421:231–237.

16. Simmer F, Moorman C, van der Linden AM, Kuijk E, van den Berghe PV, Kamath RS, Fraser AG, Ahringer J, Plasterk RH. Genome-wide RNAi of *C. elegans* using the hypersensitive *rrf-3* strain reveals novel gene functions. PLoS Biol 2003;1:E12.

17. Kraev A, Kraev N, Carafoli E. Identification and functional expression of the plasma membrane calcium ATPase gene family from *Caenorhabditis elegans*. J Biol Chem 1998;274:4254–4258.

18. Strehler EE, Zacharias DA. Role of alternative splicing in generating isoform diversity among plasma membrane calcium pumps. Phys Rev 2001;81:21–50.

19. Toyoshima C, Nomura H, Sugita Y. Structural basis of ion pumping by Ca^{2+}-ATPase of sarcoplasmic reticulum. FEBS 2003;555:106–110.

20. Treusch S, Knuth S, Slaugenhaupt SA, Goldin E, Grant BD, Fares H. *Caenorhabditis elegans* functional orthologue of human protein h-mucolipin-1 is required for lysosome biogenesis. Proc Natl Acad Sci U S A 2004;101:4483–4488.

21. Grant B, Zhang Y, Paupard MC, Lin SX, Hall DH, Hirsh D. Evidence that RME-1, a conserved *C. elegans* EH-domain protein, functions in endocytic recycling. Nat Cell Biol 2001;3:573–579.

22. Greener T, Grant B, Zhang Y, Wu X, Greene LE, Hirsh D, Eisenberg E. *Caenorhabditis elegans* auxilin: a J-domain protein essential for clathrin-mediated endocytosis *in vivo*. Nat Cell Biol 2001;3:215–219.

23. Botelho RJ, Teruel M, Dierckman R, Anderson R, Wells A, York JD, Meyer T, Grinstein S. Localized biphasic changes in phosphatidylinositol-4,5-bisphosphate at sites of phagocytosis. J Cell Biol 2000;151: 1353–1368.

24. Gaidarov I, Keen JH. Phosphoinositide-AP-2 interactions required for targeting to plasma membrane clathrin-coated pits. J Cell Biol 1999;146: 755–764.

25. Ford MG, Pearse BM, Higgins MK, Vallis Y, Owen DJ, Gibson A, Hopkins CR, Evans PR, McMahon HT. Simultaneous binding of PtdIns(4, 5)P_2 and clathrin by AP180 in the nucleation of clathrin lattices on membranes. Science 2001;291:1051–1055.

26. Lin SX, Grant B, Hirsh D, Maxfield FR. Rme-1 regulates the distribution and function of the endocytic recycling compartment in mammalian cells. Nat Cell Biol 2001;3:567–572.

27. Patton A, Knuth S, Schaheen B, Dang H, Greenwald I, Fares H. Endocytosis function of a ligand-gated ion channel homolog in *Caenorhabditis elegans*. Curr Biol 2005;15:1045–1050.

28. Rotem-Yehudar R, Galperin E, Horowitz M. Association of insulin-like growth factor 1 receptor with EHD1 and SNAP29. J Biol Chem 2001; 276:33054–33060.

29. Rolls MM, Hall DH, Victor M, Stelzer EH, Rapoport TA. Targeting of rough endoplasmic reticulum membrane proteins and ribosomes in invertebrate neurons. Mol Biol Cell 2002;13:1778–1791.

30. Kellermayer MS, Aiello DP, Misea A, Bedwell DM. Extracellualr Ca^{2+} sensing contributes to excess Ca^{2+} accumulation and vacuolar fragmentation in a pmr1Delta mutant of *S. cerevisiae*. J Cell Sci 2003;116: 1637–1646.

31. Grant B, Hirsh D. Receptor-mediated endocytosis in the *Caenorhabditis elegans* oocyte. Mol Biol Cell 1999;10:4311–4326.

32. Haaker H, Racker E. Purification and reconstitution of the Ca2+-ATPase from plasma membrane of pig erythrocytes. J Biol Chem 1979; 254:6598–6602.

33. Wanaverbecq N, Marsh SJ, Al-Qatari M, Brown DA. The plasma membrane calcium-ATPase as a major mechanism for intracellular calcium regulation in neurones from the rat superior cervical ganglion. J Physiol 2003;550:83–101.

34. Pande J, Mallhi KK, Sawh A, Szewczyk MM, Simpson F, Grover AK. Aortic smooth muscle and endothelial plasma membrane Ca^{2+} pump isoforms are inhibited differently by the extracellular inhibitor caloxin 1b1. Am J Physiol Cell Physiol 2006;290:C1341–C1349.

35. Kozel PJ, Friedman RA, Erway LC, Yamoah EN, Liu LH, Riddle T, Duffy JJ, Doetschman T, Miller ML, Cardell EL, Shull GE. Balance and hearing deficits in mice with a null mutation in the gene encoding plasma membrane Ca^{2+}-ATPase isoform 2. J Biol Chem 1998;273:18693–18696.

36. Street VA, McKee-Johnson JW, Fonseca RC, Tempel BL, Noben-Trauth K. Mutations in a plasma membrane Ca^{2+}-ATPase gene cause deafness in deafwaddler mice, Nat Genet 1998;19:390–394.

37. Takahashi K, Kitamura K. A point mutation in a plasma membrane Ca^{2+} ATPase gene causes deafness in Wriggle Mouse Sagami. Biochem Biophys Res Commun 1999;261:773–778.

38. Yamoah EN, Lumpkin EA, Dumont RA, Smith PJ, Hudspeth AJ, Gillespie PG. Plasma membrane Ca^{2+}-ATPase extrudes Ca^{2+} from hair cell stereocilia. J Neurosci 1998;18:610–624.

39. Reinhardt TA, Lippolis JD, Shull GE, Horst RL. Null mutation in the gene encoding plasma membrane Ca^{2+}-ATPase isoform 2 impairs calcium transport into milk. J Biol Chem 2004;279:42369–42373.

40. Cousin MA. Synaptic vesicle endocytosis: calcium works overtime in the nerve terminal. Mol Neurobiol 2000;22:115–128.

41. Lin HC, Moore MS, Sanan DA, Anderson RGW. Reconstitution of coated pit budding from plasma membranes. J Cell Biol 1991;114: 881–891.

42. Takahashi Y, Smith JD. Cholesterol efflux to apolipoprotein AI involves endocytosis and resecretion in a calcium-dependent pathway. Proc Natl Acad Sci U S A 1999;96:11358–11363.

43. von Gersdorff H, Matthews G. Inhibition of endocytosis by elevated internal calcium in a synaptic terminal. Nature 1994;370:652–655.

44. Miyata Y, Nishida E, Koyasu S, Yahara I, Sakai H. Regulation by intracellular Ca^{2+} and cyclic AMP of the growth factor-induced ruffling membrane formation and stimulation of fluid-phase endocytosis and exocytosis. Exp Cell Res 1989;181:454–462.

45. Korc M, Matrisian LM, Magun BE. Cytosolic calcium regulates epidermal growth factor endocytosis in rat pancreas and cultured fibroblasts. Proc Natl Acad Sci U S A 1984;81:461–465.

46. Cousin MA, Robinson PJ. Ca^{2+} influx inhibits dynamin and arrests synaptic vesicle endocytosis at the active zone. J Neurosci 2000;20: 949–957.

47. Cousin MA, Robinson PJ. The dephosphins: dephosphorylation by calcineurin triggers synaptic vesicle endocytosis. Trends Neurosci 2001; 24:659–665.

48. Murthy KS, Zhou H, Huang J, Pentyala SN. Activation of PLC-delta1 by Gi/o-coupled receptor agonists. Am J Physiol Cell Physiol 2004; 287: 1679–1687.

49. Carvou N, Norden AG, Unwin RJ, Cockcroft S. Signalling through phospholipase C interferes with clathrin-mediated endocytosis. Cell Signal 2007;19:42–51.

50. Davis MW, Hammarlund M, Harrach T, Hullett P, Olsen S, Jorgensen EM. Rapid single nucleotide polymorphism mapping in *C. elegans*. BMC Genomics 2005; 6:118.

51. Loria PM, Hodgkin J, Hobert O. A conserved postsynaptic transmembrane protein affecting neuromuscular signaling in *Caenorhabditis elegans*. J Neurosci 2004;24:2191–2201.

52. Miyabayashi T, Palfreyman MT, Sluder AE, Slack F, Sengupta P. Expression and function of members of a divergent nuclear receptor family in *Caenorhabditis elegans*. Dev Biol 1999;215:314–331.